Meteoritics & Planetary Science 38, Nr 10, 1437–1450 (2003)
Abstract available online at http://meteoritics.org

The clay mineralogy of sediments related to the marine Mjølnir impact crater

Henning DYPVIK,[1*] Ray E. FERRELL, Jr.,[2] and Pål T. SANDBAKKEN[3]

[1]Department of Geosciences, University of Oslo, P.O.Box 1047, N-0316 Oslo, Norway
[2]Department of Geosciences, Louisiana State University, Baton Rouge, Louisiana 70803, USA
[3]Statoil ASA, UPN TO SF, RESU-SFC, B4, FV, N-4035 Stavanger, Norway
[*]Corresponding author. E-mail: henning.dypvik@geo.uio.no

(Received 07 July 2003; revision accepted 22 September 2003)

Abstract–The 40 km diameter Mjølnir Crater is located on the central Barents Sea shelf, north of Norway. It was formed about 142 ± 2.6 Myr ago by the impact of a 1–2 km asteroid into the shallow shelf clays of the Hekkingen Formation and the underlying Triassic to Jurassic sedimentary strata.

A core recovered from the central high within the crater contains slump and avalanche deposits from the collapse of the transient crater and central high. These beds are overlain by gravity flow conglomerates, with laminated shales and marls on top. Here, impact and post-impact deposits in this core are studied with focus on clay mineralogy obtained from XRD decomposition and simulation analysis methods. The clay-sized fractions are dominated by kaolinite, illite, mixed-layered clay minerals and quartz. Detailed analyses showed rather similar composition throughout the core, but some noticeable differences were detected, including varying crystal size of kaolinite and different types of illites and illite/smectite. These minerals may have been formed by diagenetic changes in the more porous/fractured beds in the crater compared to time-equivalent beds outside the crater rim.

Long-term post-impact changes in clay mineralogy are assumed to have been minor, due to the shallow burial depth and minor thermal influence from impact-heated target rocks. Instead, the clay mineral assemblages, especially the abundance of chlorite, reflect the impact and post-impact reworking of older material. Previously, an ejecta layer (the Sindre Bed) was recognized in a nearby well outside the crater, represented by an increase in smectite-rich clay minerals, genetically equivalent to the smectite occurring in proximal ejecta deposits of the Chicxulub crater. Such alteration products from impact glasses were not detected in this study, indicating that little, if any, impact glass was deposited within the upper part of the crater fill. Crater-fill deposits inherited their mineral composition from Triassic and Jurassic sediments underlying the impact site.

INTRODUCTION

Clay Minerals and Impacts

Clay mineral associations may reveal many aspects of the geological history of fine-grained sediments if the multiple processes and factors controlling clay composition can be unraveled. For more than 50 yr, largely due to the pioneering work of Georges Millot and his students, sedimentologists have known that clay minerals may be directly precipitated from aqueous solutions (neoformation), inherited from primary rocks (inheritance), degraded by weathering processes (degradation), or rejuvenated and transformed during diagenesis (aggradation). In modern literature, many investigations describe modifications during deposition in varied sedimentary environments, variation in detrital clay assemblages as a result of climate change and varying rates of erosion due to tectonism, modifications due to shifting oceanic circulation patterns, and alterations due to pedogenesis and diagenesis. The mineral assemblage may be the product of a dominant process but is most frequently influenced by a combination of multiple factors.

A recent review by Ortega-Huertas et al. (2002) documented how changes in clay mineral content of the Cretaceous-Tertiary boundary clays around the globe produce a pattern supporting a major catastrophic event. Distance from the Chicxulub crater is the main factor governing the lithology, thickness, and mineralogical and chemical composition of the deposits. At proximal sites (within 600 km of the impact site), silicate-rich deposits from the ejecta blanket, a carbonate megabreccia, and complex clastics deposited from gravity flows, tsunami, and landslides are overlain by additional ballistically-transported debris and melt spherules. In most of these deposits, highly crystalline

smectite produced by post-depositional alteration is the only evidence of the original glasses and spherules (Debrabant et al. 1999; Kettrup et al. 2000). In NE Mexico, local conditions have produced a chlorite-rich clay assemblage (Mata et al. 2001). Further away, spherical and oval-shaped spherules marking the ejecta layer are overlain by deposits from the fireball layer. The smectite produced by their alteration varies from Fe-rich to Ca-rich depending on the original nature of the glass (Martinez-Ruiz et al. 2001). Still further away (more than 1000 km?) the classic two-layer continental sequence reported by Pollastro and Bohor (1993) can be recognized. Kaolin minerals have formed from silicic glasses associated with the ejecta layer. The overlying fireball layer deposits are, in the K/T, mostly altered to smectite. At more distal locations, such as in Denmark, a single, thin laminated layer formed by fireball deposits is mostly composed of Mg-rich smectite enriched in platinum group elements (Smit 1999), although Elliot (1993) believes that the smectite at Stevns Klint in Denmark is of volcanic origin. In some locations, this simple suite is complicated by the influx of locally-derived kaolin and other clays, or changed by tectonism-induced diagenesis (Robert and Chamley 1990; Ortega-Huertas et al. 1998). Variable clay content is often the only evidence for the original composition of the glassy ejecta, and clay minerals may be used to differentiate ejecta layer, fireball layer, and lowermost Danian post impact-deposits.

Dypvik and Ferrell (1998) reported clay mineral changes associated with deposits formed by the Late Jurassic (Ryazanian, early Berriasian) Mjølnir bolide impact in shallow marine shelf sediments (lower part of the Hekkingen Formation) of Volgian to Ryazanian age (core 7430/10-U-01, 30 km outside the Mjølnir crater rim; Fig. 1). Their use of profile decompostion, simulated diffraction patterns, and statistical fitting techniques provided the means to recognize several varieties of illite, smectite, chlorite, kaolinite, and mixed-layered materials in the X-ray diffraction patterns of the sediments from a core obtained about 30 km N-NE of the Mjølnir crater rim. In this marine section, deposits from the ejecta layer (Sindre Bed) were recognized by the increased abundance of a randomly-interstratified smectite/illite containing 85% smectite layers. This smectite is genetically equivalent to the smectite occurring in proximal deposits bordering the Chicxulub crater but is more iron-rich and contains more illite layers than the younger Chicxulub materials. No clay minerals related to fireball deposits were recognized.

The present study compares the clay mineral composition of deposits in the central core of the Mjølnir impact with the earlier results of Dypvik and Ferrell (1998) to gain more insight on the processes controlling the clay mineral composition of impact-related deposits. New data on the sediments within the crater, sediments that may be less diluted by mixing of materials from several sources in the ejecta curtain, are presented.

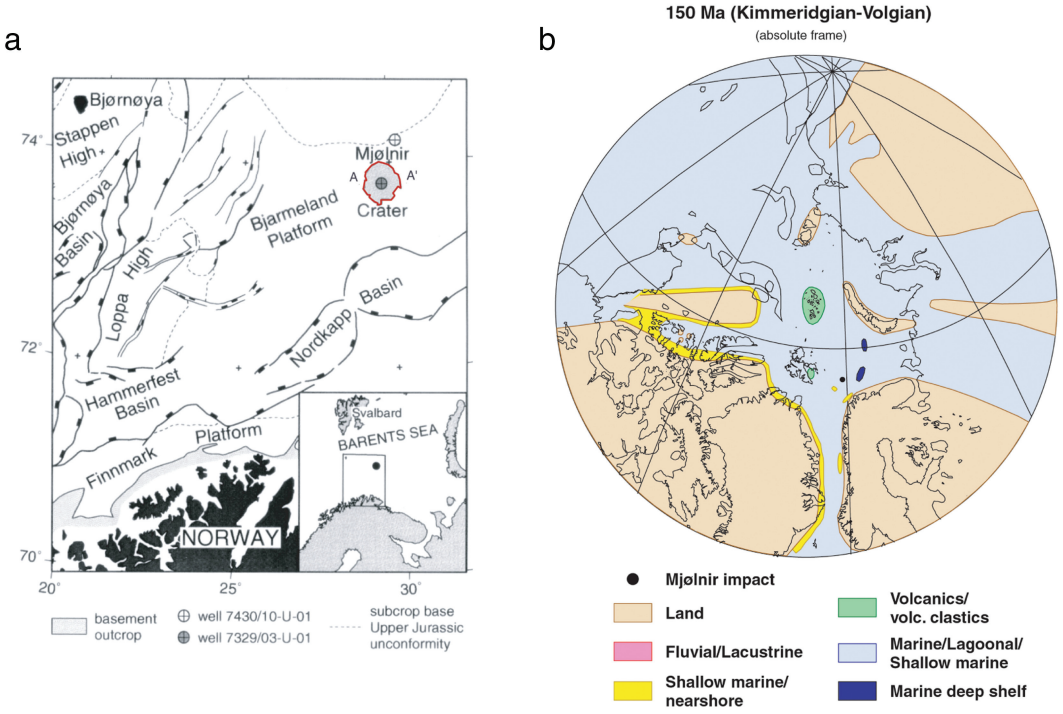

Fig. 1. a) Location map of the Barents Sea area illustrating the location of the Mjølnir crater and the examined drill cores (modified from Tsikalas et al. [1998]); b) paleogeographical reconstruction of the Barents Sea area at the time of the Mjølnir impact.

Location

The Mjølnir impact structure is located at 73°48′ N, 29°40′ E on the central Barents Sea shelf (Fig. 1), at a water depth of around 350 m and beneath a 50 to 400 m-thick cover of younger sediments (Gudlaugsson 1993; Dypvik et al. 1996). The bolide struck at the Volgian-Ryazanian boundary (early Berriasian) (*Berriasella-jacobi* zone) 142 ± 2.6 Myr ago (Smelror et al. 2001b). At that time, Svalbard was located north of North Greenland, the North Atlantic was just beginning to open, and large parts of the paleo-Arctic were covered by a shallow epicontintal sea (Fig. 1). In this sea, the Mjønir impactor, about 1.5–2.0 km in diameter (Tsikalas et al. 1999), created a 40 km crater and huge tsunami that spread around the paleo-Arctic and severely disturbed both sea bed and coastal areas (Dypvik et al. Forthcoming).

The Mjølnir Crater is a complex crater composed of a 12 km-wide outer zone, including a marginal fault zone and a modestly elevated ring, a 4 km-wide annular depression, and an 8 km diameter central high. Seismic mapping shows that an 850–1400 km^3 disturbed sediment volume is connected with crater formation (Tsikalas et al. 1998). In their numerical simulation, Shuvalov et al. (2002) demonstrated that the major part of the crater formation (compression, excavation, and collapse) phase took place within 5 min and that the sea did not return permanently to the location for about 20 min. During that time, parts of the sea bed were on fire (Wolbach et al. 2001). The central high may have formed a prominent island for a few 100 years after the impact and return of the sea.

The 121 m Mjølnir core (7329/03-U-01) was drilled (by SINTEF/IKU/The Mjølnir Group, in August 1998) at the edge of the central high (Fig. 2). The lithology and stratigraphy of the interval from 50 to approximately 110 m beneath the sea floor are illustrated in Fig. 3. The sediments can be divided into the Ragnarok, Hekkingen, and Klippfisk formations (Dypvik et al. Forthcoming). The lowermost section, from 171.08 to 88.35 m (unit I of the Ragnarok Formation), contains slumped Middle Triassic to Middle Jurassic sediments, probably formed during or just after the uplift of the central high. These sediments are succeeded by different types of gravity flow deposits representing different stages in the erosion and collapse of the central high. The conglomerate of unit IIa (0.92 m thick) of the Ragnarok Formation is a composite of 3 debris flow deposits, while the 11.70 m-thick unit IIb consists of mud flow/autobrecciated clay- and siltstones (Fig. 3). Unit IIb could represent a debris avalanche (cf., Palmer et al. 1991), that developed into a debris flow. In Palmer et al. (1991), the debris avalanche was triggered by the pressure differences and erosion related to a powerful tsunami. Tsunami-induced dynamic loading on the flanks of the central high could cause so-called "explosive" (due to high pressure differences) liquefaction and subsequent gliding of the liquefied and brecciated mass (autobrecciation). Unit IIb most likely represents the effect of one of the later tsunami, probably generated by resurge into the crater (Dypvik et al. Forthcoming). Its upper part most probably was deposited from suspension, as it is highly enriched in the very light remains of *Tasmanites* algae, each about 1 mm in diameter (Bremer et al. 2003).

The uppermost part of the Ragnarok Formation is unit IIc, which is composed of several sequences of light grey debris flow conglomerates succeeded by thin turbidites. This unit is 1.68 m thick, and the individual debris flow/turbidite couples average about 40 cm in thickness (Fig. 3). Dark grey, finely-laminated fossil-rich shales of the Hekkingen Formation overlay unit IIc. The Hekkingen Formation represents anoxic to hypoxic depositional conditions rich in sulphides, fossils, and organic matter. The Hekkingen Formation shales can contain more than 20% TOC, and they represent normal Upper Jurassic sedimentation in the area. These deposits are similar to those that were accumulating in the area before the impact (Dypvik et al. Forthcoming; Smelror et al. 2001a; Leith et al. 1993).

In a recent study of shocked particle (quartz and feldspar) mineralogy of the Mjølnir core, Sandbakken (2002) found planar fractures (PF) and possibly also some planar

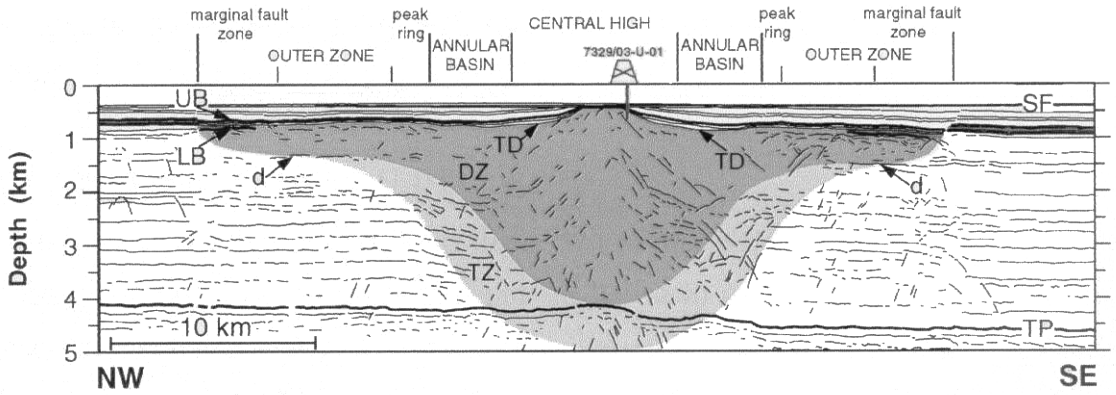

Fig. 2. An interpreted seismic section across the Mjølnir Crater illustrating the so-called inverted sombrero style. The drill core location is indicated. Modified from Shuvalov et al. (2002).

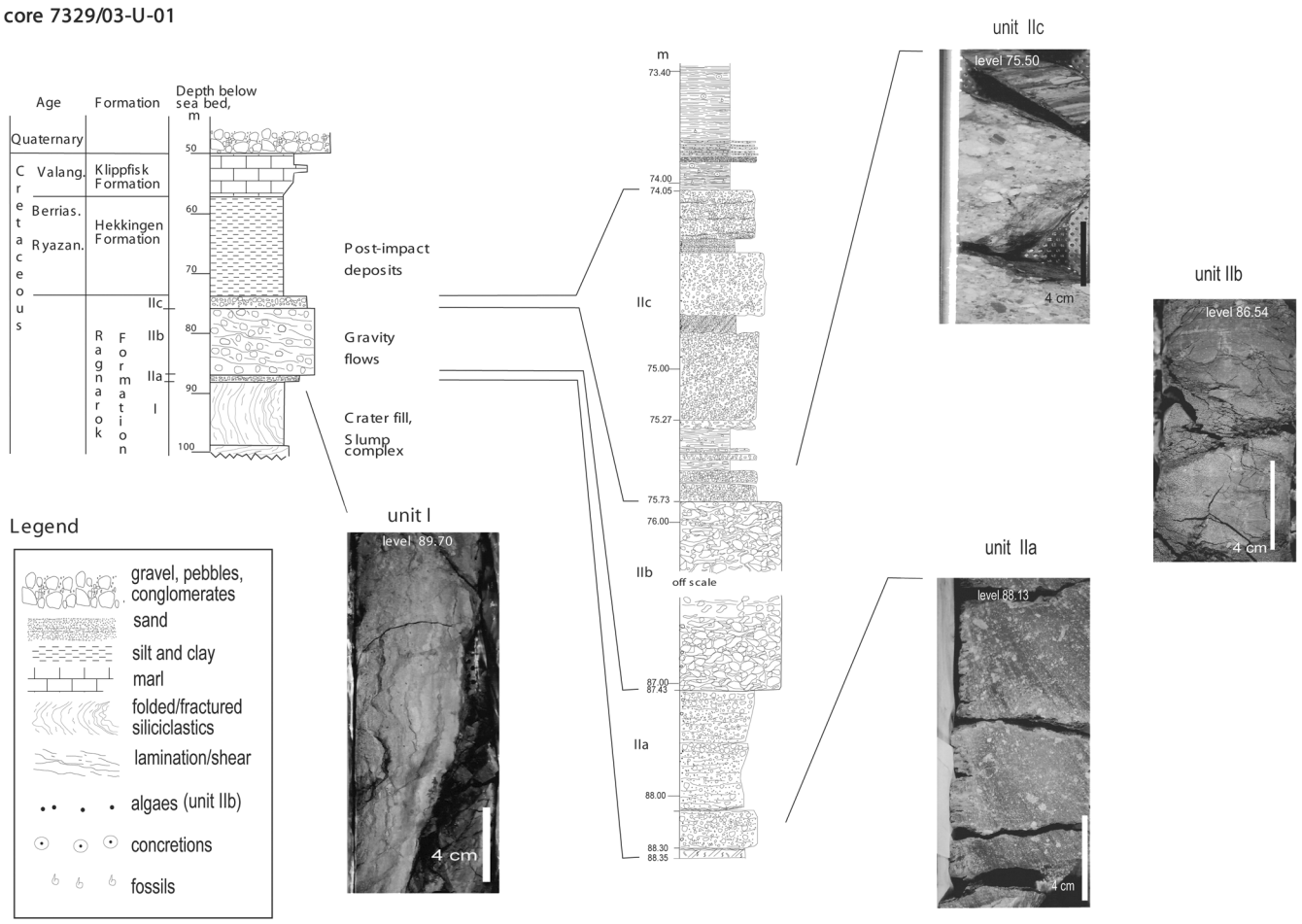

Fig. 3. General sedimentologic and stratigraphic logs from the Mjølnir drill core 7329/03-U-01 accompanied by typical photos of units I, IIa, IIb, and IIc.

deformation features (PDF) throughout major parts of the Ragnarok Formation. These results suggest that the sediments probably encountered pressures up to 20 GPa. According to Sandbakken (2002) and Shuvalov et al. (2002), temperatures reached several thousand degrees at the impact site. So far, however, no melt or glass particles have been found in the Mjølnir core. Shuvalov and Dypvik (Forthcoming) and Tsikalas (personal communication, 2003) demonstrated that the impact orientation was from the S-SW, allowing asymmetrical distribution of ejecta toward the N-NE and North Russia/Siberia.

METHODS

Whole rock samples were crushed in an agate mortar to produce a fine powder and were pressed to form randomly-oriented pellets for X-ray diffraction analysis (Philips X'Pert MPD). A numerical estimate of mineral abundances (semiquantitative) in the whole rock samples was derived from simple peak height percentage calculations without mineral reference intensity correction factors. Samples for clay mineral analysis (<2 μm) were obtained by extracting the upper 5 cm of a slurry that had been allowed to settle for 3 hr 10 min at 22°C. Oriented films for XRD were produced by smearing the clay paste on glass plates and were then analyzed in the air-dried, ethylene glycol (EG) saturated state (vapor phase saturation overnight in a dessicator) after heating to 300°C and 550°C for 1 hr. XRD patterns were obtained with a Siemens (Bruker) D5000 diffractometer employing a Cu tube operated at 40 kV and 30 mA. Data were recorded by counting for 2 sec at 0.04° 2θ steps over the interval from 2° 2θ to 50° 2θ, as detailed in Dypvik and Ferrell (1998).

Quantitative representation (QR of Hughes et al. 1994) of the clay minerals in the assemblage was determined by a least-squares comparison of the laboratory patterns from EG-saturated samples with NEWMOD simulated patterns (Huang et al. 1993; Aparicio and Ferrell 2001). The program systematically varies the fractional multipliers for each simulated pattern until the sum of the library patterns matches the observed X-Ray intensity at each 2θ point. The fractional contributions after normalizing to 1.0 are proportional to the weight fraction of the mineral in the crystalline portion of the clay fraction. These estimates of abundance do not meet the

rigorous demands of a quantitative phase analysis but provide internally consistent, semi-quantitative numerical estimates of changes in composition.

The parameters used in the computer simulation are summarized in Table 1. The nomenclature for the mixed-layered materials is derived from the names of the layer types used in the simulation, with the exception of those combinations employing a chlorite layer (CIR1 and CIR2). Material containing 60–80% illite layers (dimica) with a dismectite represents an illite-rich illite/smectite, but we have referred to combinations of chlorite and illite as mixed-layered vermiculite/illite. This departure from the norm was brought about because we had to remove the interlayer hydroxide sheet from the standard trichlorite to match actual peak intensities. Standard vermiculite layers would not produce a reasonable fit. The actual material swells to 14Å with EG and partially collapses with heat treatment similar to hydroxy interlayered vermiculite.

RESULTS

Whole Rock Mineralogy

The whole-rock XRD average results (semiquantitative) (Table 2) display some stratigraphic variations in mineral abundance. The major differences in the formations and units are illustrated in the bar graphs of Fig. 4. Units I and II of the Ragnarok Formation are similar, while the Hekkingen Formation (Fig. 5) samples display a very different mineral assemblage. The Hekkingen Formation samples in this

Table 1. Clay mineral specifications of clay minerals in the simulations (NEWMOD).

Symbol and description	Layer types (fraction)	Ordering	Layer 1 composition	Layer 2 composition	Crystallite thickness
KAO07 Medium-crystallite-kaolinite	Kaolinite	Pure	Fixed	Fixed	Low N = 7 High N = 14
KAO11 Fine-crystallite-kaolinite	Kaolinite	Pure	Fixed	Fixed	Low N = 3 High N = 7
ILL05 Medium-crystallite, no Fe, K-depleted illite	Dimica	Pure	0.0 Fe 0.5 K	Same	Low N = 3 High N = 14
ILL11 Medium-crystallite, moderate Fe illite	Dimica	Pure	1.0 Fe 1.0 K	Same	Low N = 3 High N = 14
ILLUT Medium-crystallite, low Fe illite	Dimica	Pure	0.2 Fe 1.0 K	Same	Low N = 3 High N = 14
CH20 Medium-crystallite, Fe-rich chlorite	Di/di chlor	Pure	1.0 Sil Fe 1.0 Hyd Fe 0.9 Hyd	Same	Low N = 5 High N = 14
TTCH511 Medium-crystallite, Fe-rich chlorite	Tri/tri chlor	Pure	1.2 Sil Fe 2.1 Hyd Fe 0.9 Hyd	Same	Low N = 7 High N = 14
IS6R1 Fine-crystallite, illite-rich IS	Dimica (0.6) Dismec 2-gly (0.3)	R = 1	0.5 Fe 0.9 K	0.5 Fe	Low N = 5 High N = 11
IS7R1 Fine-crystallite, illite-rich IS	Dimica (0.7) Dismec 2-gly (0.2)	R = 1	0.5 Fe 0.9 K	0.5 Fe	Low N = 5 High N = 11
IS8R1 Fine-crystallite, illite-rich IS	Dimica (0.8) Dismec 2-gly (0.1)	R = 1	0.5 Fe 0.9 K	0.5 Fe	Low N = 5 High N = 11
IS9R1 Fine-crystallite, illite-rich IS	Dimica (0.9) Dismec 2-gly (0.1)	R = 1	0.5 Fe 0.9 K	0.5 Fe	Low N = 5 High N = 11
CIR1 Medium-crystallite, low Fe, vermiculite/illite	Tri/tri chlor (0.5) Dimica (0.5)	R = 1	0.2 Sil Fe 0.0 Hyd Fe 0.0 Hyd	0.2 Fe 0.9 K	Low N = 4 High N = 14
CIR2 Medium-crystallite, low Fe, vermiculite/illite	Tri/tri chlor (0.6) Dimica (0.4)	R = 1	0.2 Sil Fe 0.0 Hyd Fe 0.0 Hyd	0.2 Fe 0.9 K	Low N = 4 High N = 14

Table 2. The average qualitative whole-rock XRD proportions of Hekkingen Formation sediment (5 samples) and of the 4 units of the Ragnarok Formation (unit I, 6 samples; unit IIa, 3 samples; unit IIb, 7 samples; unit IIc, 6 samples). Semiquantitative data.

Sample	14Å Chlorite	16–17Å Smectite	10–13Å Mixed layer min.	10Å Illite	7Å Kaolinite	4.26Å Quartz	3.20Å Plagioclase	3.03Å Calcite	2.89Å Dolomite	2.79Å Siderite	2.71Å Pyrite
Hekkingen	3	17	2	22	25	16	2	1	1	3	8
IIc	9	1	5	19	49	9	5	2	0	1	2
IIb	7	1	2	17	57	7	3	1	0	2	1
IIa	9	1	3	23	52	6	4	0	0	1	1
I	9	1	3	24	49	5	4	5	0	1	1

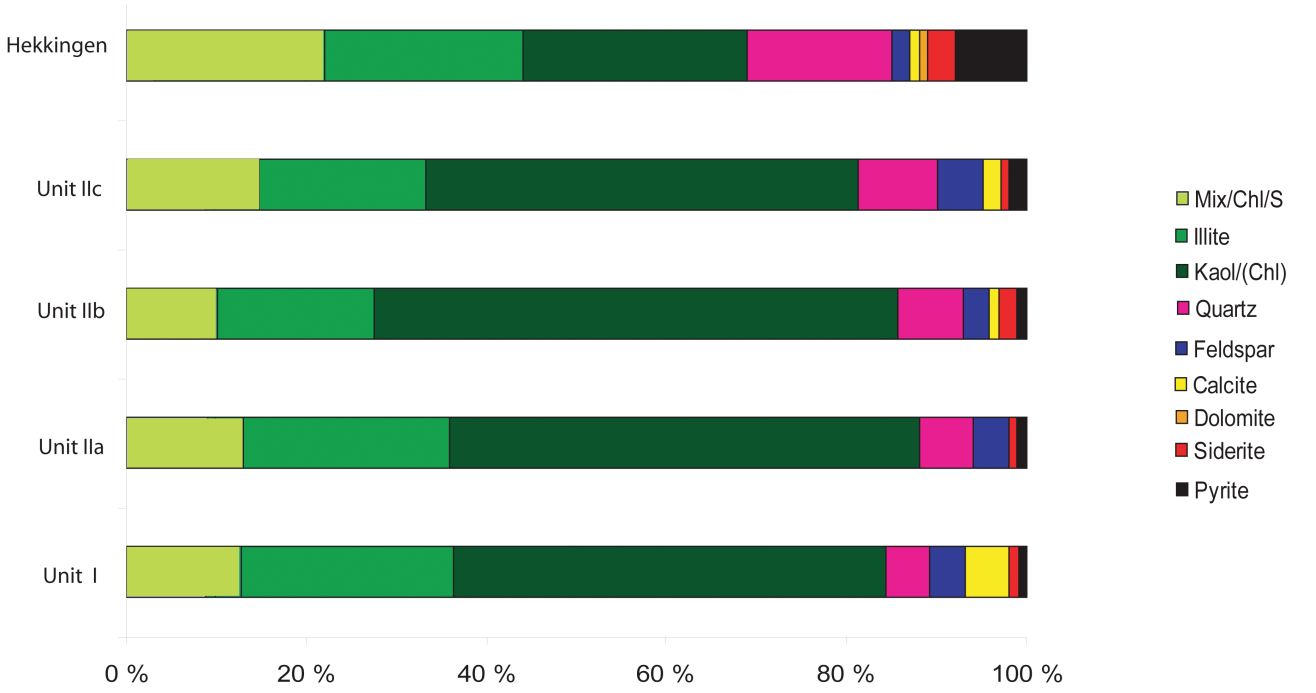

Fig. 4. The average (whole rock) semiquantitative mineralogical distributions in the Hekkingen Formation and units I, IIa, IIb, and IIc of the Ragnarok Formation. Mix/Ch/Sme includes mixed layered clayminerals, chlorite, and smectite. Kaol/(Chl) is based on the 7Å peak, which is mainly kaolinite but also includes some chlorite.

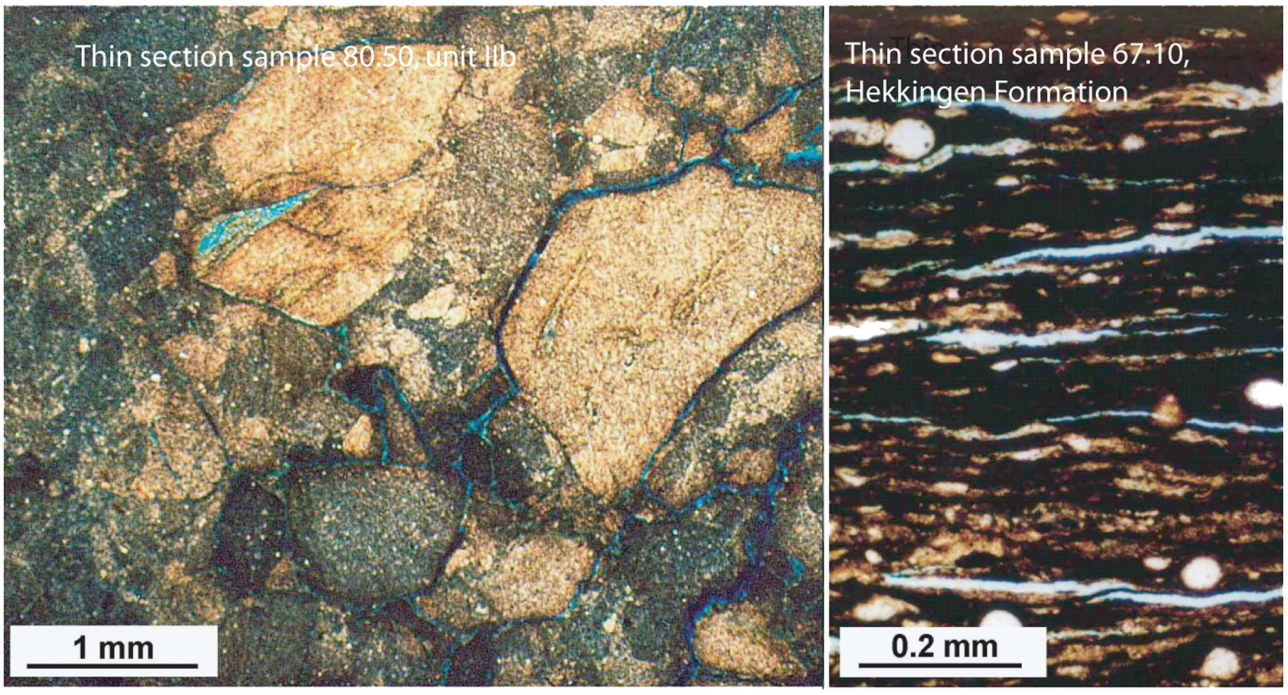

Fig. 5. Thin section micrographs of typical samples from the Hekkingen Formation and unit IIb claystone of the Ragnarok Formation. In the Hekkingen sample on the right, the finely laminated, organic-rich laminae are seen with light grains of spherical algae, while up to several mm-wide intraformational mud-flakes dominate in the often grain-supported structure of unit IIb claystones on the left.

Mjølnir core (7329/03-U-01) are similar to the Hekkingen Formation assemblage published earlier by Dypvik and Ferrell (1998) (drill core 7430/10-U-01) (Fig. 1), except for their slightly higher feldspar abundances. Within units I, IIa, and IIb, thin section analyses show siderite to be more abundant than in units above (Sandbakken 2002), but this is not displayed in the semiquantitative XRD presented here (Table 2). In thin section, siderite more or less disappears in unit IIc, while pyrite and calcite increase in relative abundance. Unit IIc contains smaller quantities of 7Å (kaolinite plus chlorite) and 14Å (chlorite) components than the units below (Table 2). Higher pyrite values are observed in units IIb and IIc and the Hekkingen Formation than in units I and IIa.

Clay Mineralogy

General aspects of the stratigraphic variations in the clay assemblages from depths of 60–100 m in the Mjølnir core are illustrated in the composite XRD patterns of Fig. 6. The lower pattern (A) is the sum of individual XRD results for 4 samples from the slump complex (unit I of the Ragnarok Formation). It is characterized by distinct peaks at 6.2° (14Å), 8.8° (10Å), and 12.4° (7Å) 2θ, representing chlorite, illite, and combined chlorite and kaolinite, respectively. Clay-sized quartz is represented by the peak at 20.8° 2θ (4.26Å) 2θ. Broad bands near 6.2° and 18° 2θ suggest the presence of mixed-layered clay minerals (Mx). The small peak near 28° 2θ is attributed to clay-sized feldspar (Fspar). Other peaks are multiple reflections from the major clay minerals. Pattern B represents samples from the coarse-grained conglomerate unit IIa (0.92 m thick). The XRD peak positions and intensities are almost the same as in the lower composite (A), but the broad bands representing mixed-layered clays are not as obvious. The composite pattern (C) from the center of the 11.7 m-thick autobrecciation/mud flow sequence (unit IIb) also shows little difference in the types of minerals present. In the overlying coarse-grained unit IIc, the composite XRD pattern from this 1.68 m-thick interval (D) is similar to those from units I and II, but the peak intensity of the first chlorite peak is lower, and weak, broad diffraction bands surround it. The presence of kaolinite and chlorite is confirmed by the double peak appearing at approximately 25° 2θ. In the 16.85 m-thick interval of dark grey shale of the Hekkingen Formation that formed after deposition had returned to "normal" pre-impact conditions (Dypvik et al. Forthcoming), the first chlorite peak is almost absent (E) and a broad band appears in the area of 5° 2θ, representing smectite or smectite-rich mixed-layered clay minerals (Smect). The peak at 29.4° 2θ is clay-sized calcite (Cc).

More detailed representation of the clay mineral changes detected in the 60–100 m depth interval of the Mjølnir core are presented in Figs. 7 and 8. The data points represent the relative weight fractions of the identified clay minerals as derived from simulated clay mineral patterns produced with

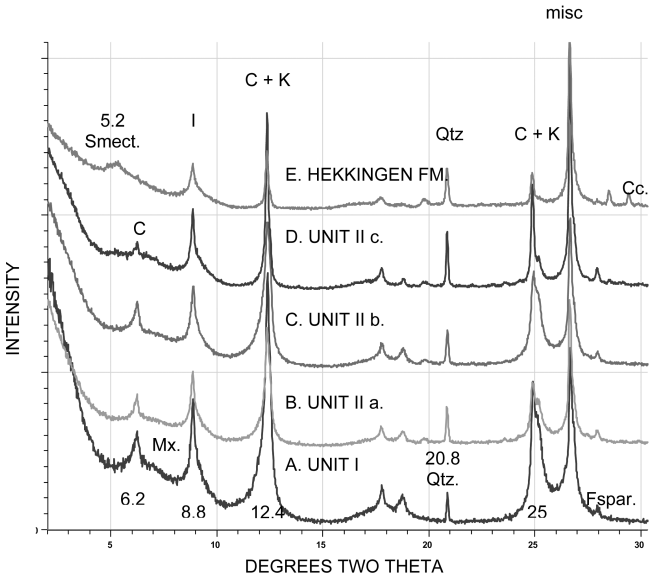

Fig. 6. Composite XRD patterns of bulk samples of the clay fraction from the Hekkingen and Ragnarok formations, units I, IIa, IIb, and IIc. EG-solvated state. C = chlorite, I = illite, K= kaolinite, Qtz = quartz, misc = miscellaneous composite peak with, e.g., clay minerals and quartz. See text for pattern descriptions.

the parameters in Table 1. Three varieties of simulated illite were used to represent the actual illite present in the samples (Tables 1 and 3). These and the other detailed mineral interpretations are best provided by this simulation approach (Aparicio and Ferrell 2001; Dypvik and Ferrell 1998). The illite (Fig. 7a) and illite/smectite (Fig. 7b) diagrams also contain points representing the qualitative calculated total quantity of illite or illite/smectite. Two samples from greater depths in the core (140 and 165 m, lower part of slump complex, not plotted in Fig. 3) have clay mineral assemblages that also fall within the range depicted for samples from the upper part of the crater fill slump complex of unit I (88–100 m).

The sum of the weight fractions for the 3 types of simulated illite are represented by the solid circles in Fig. 7. Total illite usually comprises 30 to more than 50% of the clay mineral assemblage. It is most abundant in unit IIc and the Hekkingen Formation, i.e., samples above the 75 m level. In these samples, more than 50% of the total illite can be represented by a medium-crystallite thickness, K-depleted illitic mineral, with no Fe, in the octahedral sheet (ILL05). The stratigraphic units below 75 m contain illite that can be represented by approximately equal quantities of the K-depleted illite and two other illites with more normal K contents and 0.2 or 1.0 atoms of ferric Fe in their dioctahedral sheets (ILLUT and ILL11, respectively). The iron-rich illite (ILL11) was also observed in the core outside the crater rim (Dypvik and Ferrell 1998).

The presence of varieties of R = 1 ordered illite/smectite (IS) containing 0.6–0.9 illite layers can account for some of the broad diffraction bands observed in Fig. 6. The relative

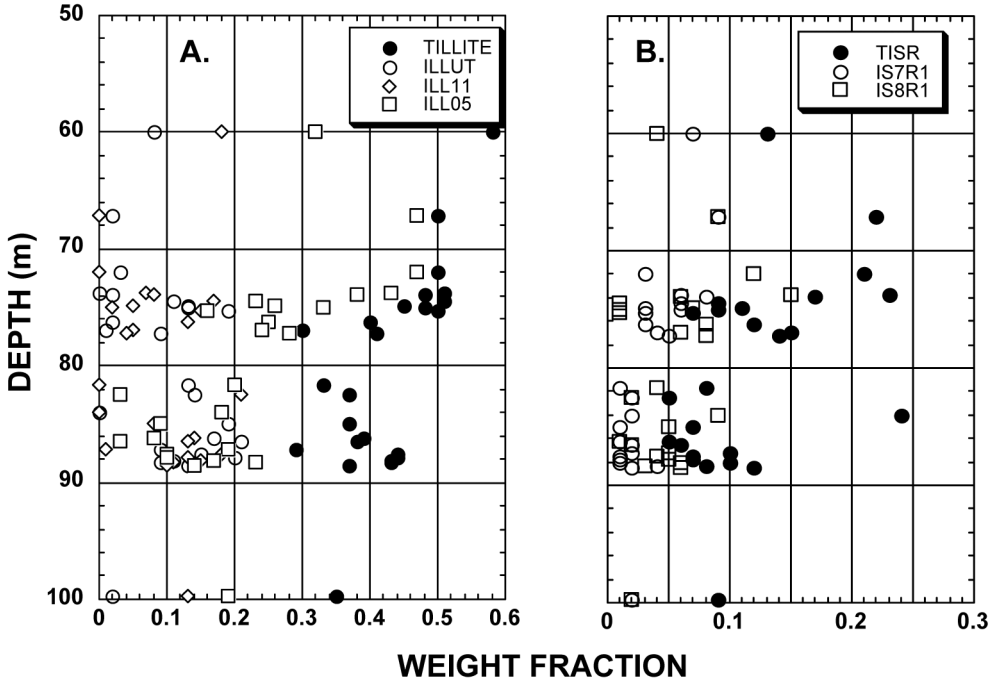

Fig. 7. Stratigraphic plots of illite and illite/smectite mineral distributions. T = total, TILLITE = total illite, TISR = total IS mixed-layered clay minerals. See Table 1 for abbreviations.

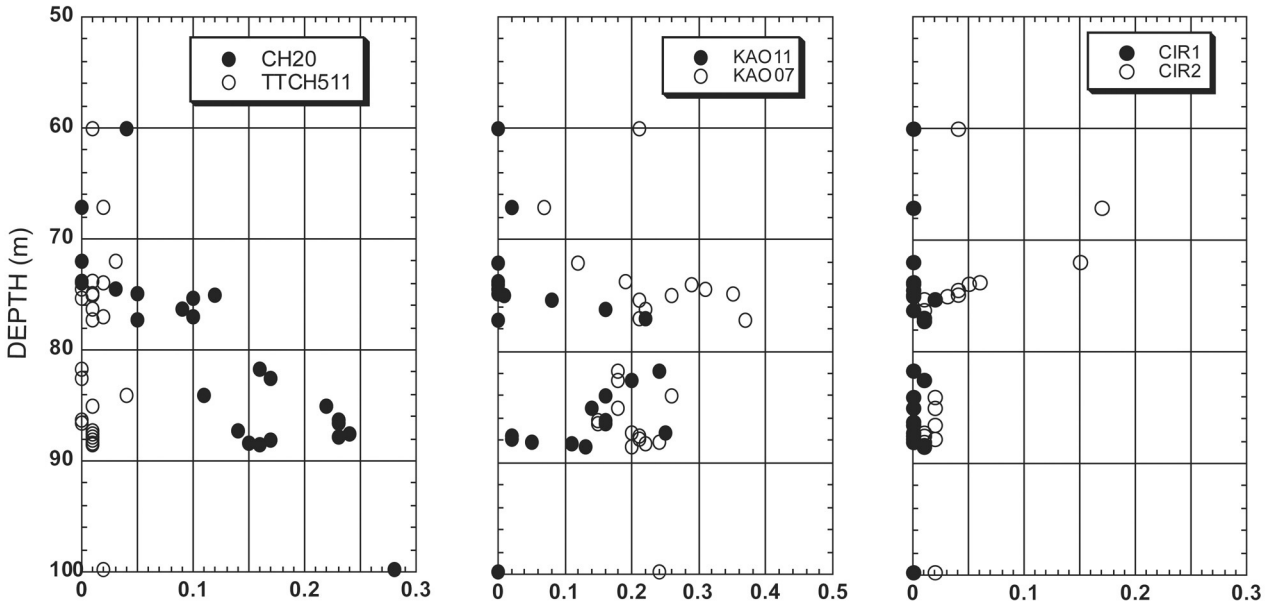

Fig. 8. Stratigraphic plots of kaolinite and chloritie mineral distributions. See Table 1 for abbreviations.

total abundance and variability of the individual IS minerals with depth in the Mjølnir core are depicted in Fig. 7. They are most abundant in the post-impact shale (Hekkingen formation) where the IS weight fraction is approximately 20%. In the lower conglomerate (unit IIa) and the overlying claystone (unit IIb), the total IS weight fraction is minor, ranging from 5–10% (75.73 to 88.35 m levels). The finely crystalline illite/smectites most commonly have 70 (IS7R1) to 80 (IS8R1) percent illite layers with 0.5 Fe out of 2.0 atoms in the octahedral sheet. No high-smectite content, mixed-layered minerals were detected.

Small quantities of chlorite are present in all samples. It is most abundant in the lower conglomerate of unit IIa and the associated claystone (unit IIb) at depths greater than the 76 m level (Fig. 8). The trioctahedral chlorite (TTCH511) is usually only a small fraction of the sample.

The kaolinite distribution is illustrated in Fig. 8. The weight fraction of medium-crystallite-size kaolinite (KAO07) forms 6–37% of the clay assemblage. It is most abundant (20–37%) in the upper conglomerate zone (unit IIc, 74.05–75.73 m). In the lower conglomerate (unit IIa, 87.43–88.35 m) and the claystone interval (unit IIb, 75.73–87.43 m), its abundance (15–25%) is about one-half that present in the upper unit. Samples from the lower units contain up to 25% fine crystallite-size kaolinite (KAO11); however, medium crystallite kaolinite is not detected in many of the samples from unit IIc or in the post-impact shale of the Hekkingen Formation.

The least abundant (usually a trace to 5% weight fraction) clay minerals are mixed-layered minerals that can be represented by simulation models containing incomplete chlorite and dimica layers (CIR1 and CIR2). These minerals are regularly stratified and low in Fe. They are identified as vermiculite/illite in Table 1. The mineral with 0.6 chlorite-like layers (CIR 2) comprises 5–17% of the clays in the post-impact dark grey shales of the Hekkingen formation (Fig. 8).

Table 3. Uncalibrated clay mineral proportions as determined by the clay mineralogical simulations. See Table 1 for abbreviations.

Stratigraphic unit	Sample depth (m)	CH20	CIR1	CIR2	ILL05	ILL11	ILLU3	IS6R1	IS7R1	IS8R1	IS9R1	KAO01	KAO11	TTCH	Sum
Hekkingen Fm.	60.00	0.04	0.00	0.04	0.32	0.18	0.08	0.01	0.07	0.04	0.01	0.00	0.21	0.01	1.01
Hekkingen Fm.	67.10	0.00	0.00	0.17	0.47	0.00	0.02	0.02	0.09	0.09	0.02	0.02	0.07	0.02	0.99
Hekkingen Fm.	72.00	0.00	0.00	0.15	0.47	0.00	0.03	0.03	0.03	0.12	0.03	0.00	0.12	0.03	1.01
Hekkingen Fm.	73.70	0.00	0.00	0.06	0.43	0.07	0.00	0.01	0.06	0.15	0.01	0.00	0.19	0.01	0.99
Hekkingen Fm.	73.90	0.00	0.00	0.05	0.38	0.08	0.02	0.02	0.08	0.06	0.02	0.00	0.29	0.02	1.02
Rag. Fm. unit IIc	74.20	0.05	0.01	0.01	0.28	0.04	0.09	0.01	0.05	0.08	0.01	0.00	0.37	0.01	1.01
Rag. Fm. unit IIc	74.40	0.03	0.00	0.04	0.23	0.17	0.11	0.02	0.06	0.01	0.00	0.00	0.31	0.00	0.98
Rag. Fm. unit IIc	74.80	0.05	0.00	0.04	0.26	0.05	0.13	0.01	0.03	0.07	0.01	0.00	0.35	0.01	1.01
Rag. Fm. unit IIc	75.00	0.12	0.00	0.03	0.33	0.02	0.13	0.01	0.06	0.01	0.01	0.01	0.26	0.01	1.00
Rag. Fm. unit IIc	75.30	0.10	0.02	0.01	0.16	0.15	0.19	0.02	0.03	0.01	0.00	0.08	0.21	0.00	0.98
Rag. Fm. unit IIb	76.20	0.09	0.00	0.01	0.25	0.13	0.02	0.01	0.03	0.08	0.01	0.16	0.22	0.01	1.02
Rag. Fm. unit IIb	77.00	0.10	0.01	0.01	0.24	0.05	0.01	0.01	0.04	0.06	0.04	0.22	0.21	0.02	1.02
Rag. Fm. unit IIb	81.68	0.16	0.00	0.00	0.20	0.00	0.13	0.01	0.01	0.04	0.03	0.24	0.18	0.00	1.00
Rag. Fm. unit IIb	82.50	0.17	0.01	0.01	0.03	0.21	0.14	0.02	0.02	0.02	0.00	0.20	0.18	0.00	1.01
Rag. Fm. unit IIb	84.00	0.11	0.00	0.02	0.18	0.00	0.00	0.02	0.02	0.09	0.11	0.16	0.26	0.04	1.01
Rag. Fm. unit IIb	85.00	0.22	0.00	0.02	0.09	0.08	0.19	0.01	0.01	0.05	0.01	0.14	0.18	0.01	1.01
Rag. Fm. unit IIb	86.20	0.23	0.00	0.00	0.08	0.14	0.17	0.02	0.01	0.01	0.00	0.16	0.15	0.00	0.97
Rag. Fm. unit IIb	86.50	0.23	0.00	0.02	0.03	0.13	0.21	0.00	0.02	0.02	0.00	0.16	0.15	0.00	0.97
Rag. Fm. unit IIb	87.20	0.14	0.00	0.01	0.19	0.01	0.09	0.01	0.02	0.05	0.02	0.25	0.20	0.01	1.00
Rag. Fm. unit IIa	87.55	0.24	0.00	0.01	0.10	0.18	0.15	0.01	0.01	0.04	0.01	0.02	0.21	0.01	0.99
Rag. Fm. unit IIa	87.80	0.23	0.00	0.02	0.10	0.13	0.20	0.01	0.01	0.05	0.01	0.02	0.21	0.01	1.00
Rag. Fm. unit IIa	88.10	0.17	0.00	0.01	0.17	0.15	0.11	0.01	0.01	0.06	0.01	0.05	0.24	0.01	1.00
Rag. Fm. unit IIa	88.30	0.15	0.01	0.01	0.23	0.11	0.09	0.01	0.04	0.03	0.01	0.11	0.22	0.01	1.03
Rag. Fm. unit I	88.50	0.16	0.01	0.01	0.14	0.10	0.13	0.01	0.02	0.06	0.03	0.13	0.20	0.01	1.01
Rag. Fm. unit I	99.77	0.28	0.00	0.02	0.19	0.13	0.02	0.02	0.02	0.02	0.02	0.00	0.24	0.02	0.98
Rag. Fm. unit I	140.00	0.17	0.00	0.02	0.17	0.01	0.15	0.01	0.03	0.04	0.01	0.21	0.18	0.00	1.00
Rag. Fm. unit I	165.50	0.19	0.00	0.00	0.18	0.09	0.14	0.01	0.01	0.03	0.01	0.16	0.16	0.00	0.98

	CH20	CIR1	CIR2	ILL05	ILL11	ILLUT	IS6R1	IS7R1	IS8R1	IS9R1	KAO07	KAO11	TTCH511
CH20	1.00												
CIR1	-0.05	1.00											
CIR2	-0.61	-0.25	1.00										
ILL05	-0.84	-0.17	0.75	1.00									
ILL11	0.33	0.21	-0.37	-0.49	1.00								
ILLUT	0.58	0.14	-0.43	-0.71	0.35	1.00							
IS6R1	-0.33	0.08	0.51	0.34	-0.05	-0.37	1.00						
IS7R1	-0.79	0.00	0.57	0.77	-0.18	-0.51	0.19	1.00					
IS8R1	-0.58	-0.19	0.54	0.63	-0.47	-0.63	0.12	0.25	1.00				
IS9R1	-0.13	-0.09	0.08	0.14	-0.51	-0.52	0.23	-0.06	0.39	1.00			
KAO07	0.40	0.14	-0.47	-0.52	-0.16	0.19	-0.26	-0.51	-0.23	0.20	1.00		
KAO11	-0.20	0.12	-0.37	0.02	0.07	-0.08	-0.12	0.14	-0.06	0.05	-0.36	1.00	
TTCH511	-0.32	-0.17	0.46	0.47	-0.44	-0.72	0.42	0.21	0.58	0.78	-0.26	0.06	1.00

Fig. 9. Correlative matrix for the clay minerals in the clay fraction mineral data (n = 28, Table 3). See Table 1 for abbreviations.

Mineralogical Associations

Simple linear correlation coefficients were calculated to assess potential interdependent relationships among the mineral abundances in the clay fraction (28 samples). Correlation coefficients (Fig. 9) with absolute values greater than 0.6 represent potentially significant associations (>40% of the variance). Positive correlations link Fe-rich chlorite (CH20) with low Fe illite (ILLUT), low Fe verm/il (CIR 2) with K-depl. illite (ILL05), low Fe verm/il (CIR2) with illite-rich IS (IS7RI), K-depl. illite (ILL05) with illite-rich IS (IS7RI), K-depl. illite (ILL05) with illite-rich IS (IS8RI), Fe-rich chlorite (TTCH511) with illite-rich IS (IS8RI), and finally, Fe-rich chlorite (TTCH511) with illite-rich IS (IS9RI) (Table 1; Fig. 9). Negative correlations link Fe-rich chlorite (CH20) with low Fe verm/il (CIR2), Fe-rich chlorite (CH20) with K-depl. illite (ILL05), Fe-rich chlorite (CH20) with illite-rich IS (IS7RI), Fe-rich chlorite (CH20) with illite-rich IS (IS8RI), K-depl. illite (ILL05) with low Fe illite (ILLUT), low Fe Illite (ILLUT) with illite-rich IS (IS8RI), and finally, low Fe illite (ILLUT) with Fe-rich chlorite (TTCH511) (Table 1; Fig. 9).

Generally, these associations are well displayed in the stratigraphic distribution of the minerals and are summarized below.

1. The samples of the Ragnarok Formation (units I and II, below the 74.05 m level) are richer in dioctahedral iron-rich chlorite (CH20), medium-crystallite low-Fe illite (ILLUT), and a moderate Fe illite (ILL11) as compared to the Hekkingen Formation samples.
2. The Hekkingen Formation contains relatively more vermiculite/illite (CIR 2), a no-Fe, K-depleted illite (ILL05), and an illite/smectite (IS8R1).

Minerals in the clay-size fraction of the samples in the crater core commonly differ from those found at the more distant location (Dypvik and Ferrell 1998). A general comparison reveals:

1. The most abundant varieties of simulated illite (ILL05) and chlorite (CH20), found in the crater core, were not identified in the study of the more distal core.
2. Other new minerals identified in the crater core include a medium crystallite, low-Fe illite (ILLUT), and two varieties of vermiculite/illite (CIR1 and CIR2).
3. Simulated minerals common to both settings include the kaolinites (KAO07 and KAO11), the medium-crystallite, low-Fe illite (ILL11 = DIMICA11), the Fe-rich chlorite (TTCH511), and varieties of illite/smectite (IS7R1 and IS8R1).

DISCUSSION

Main Mineralogy and Sedimentology

At the end of the Late Jurassic, the Mjølnir bolide hit the hypoxic (the partly anoxic) sea bed which was covered by clays and claystones of the several 100 m-thick Hekkingen Formation. At that time, euxinic bottom water conditions dominated in this part of the paleo-Barents Sea, succeeding the more ventilated (oxidized) conditions of the older siliciclastic Jurassic and Triassic beds (Worsley et al. 1988; Smelror et al. 2001a). These underlying beds were later to be exposed locally by crater excavation and the uplift and formation of the central high.

Based on examinations of the grains of shocked quartz found throughout the Ragnarok Formation, pressures up to at least 20 GPa and temperatures of several thousand degrees must have been imposed on the target rocks (Sandbakken 2002). The main phase of the impact crater formation lasted ~5 min, while the sea water permanently returned to the crater about 20 min after impact (Shuvalov et al. 2002) and normal pre-impact-type depositional conditions were re-established.

Commonly, in the early phase of crater formation, glass and melt rocks, along with impact breccias, may be formed. However, in the case of the Mjølnir impact, little melt or glass ejecta have been found so far, either in the geophysical investigations (Tsikalas et al. 1998, 1999) or in the studied cores. Glass altered to smectite has, so far, only been found in core 7430/10-U-01 located 30 km outside the crater (Dypvik and Ferrell 1998), and no glass-derived minerals have been detected in the Mjølnir core discussed here.

The sediments of the Mjølnir core represent a chaotic, slumped lower stratigraphic unit, overlain by gravity flows of the late syn- to post-impact stages. The gravity flow deposits have a mineralogy and clay mineral composition similar to the underlying Triassic and Early Jurassic units (Fig. 4), thus, clearly demonstrating their clastic, reworked origin. The post-impact return of the anoxic to sulphidic sedimentation of the Hekkingen Formation marked an important change in the depositional environment (Figs. 4 and 10). During such conditions, the characteristic acidic bottom water may percolate into underlying, porous formations where vulnerable minerals (e.g., chlorite) may quickly be altered or dissolved.

Clay Mineralogy

The clay mineral content of a sediment normally varies as a function of source terrain, depositional environment, and post-depositional/diagenetic modification (Weaver 1989). In the area of the Mjølnir Crater, the longer-term post-depositional influence is assumed to have been minor on the clay mineral content because of the rather shallow total depth of burial (<2000 m) of the impact and post-impact sediments (Tsikalas et al. 1998). This 1500–2000 m overburden was removed by Tertiary erosion (Nyland et al. 1992). The deeper formations exposed along the central high, e.g., Middle Triassic to Middle Jurassic formations, were uplifted from stratigraphic levels ~500–1000 m below the Late Jurassic impacted surface (Bremer et al. 2003). The impactites of units

I and II represent mixing associated with the bolide impact, which obliterated stratigraphic differences in the minerals originally present. This process also produced the clasts, which are major components of these conglomeratic deposits.

Three important clay mineralogical relationships have been observed in the Ragnarok Formation:

1. Units I and II display similar clay mineral contents.
2. A decrease exists in the abundance of medium-crystallite-size Fe-rich chlorite relative to kaolinite and illite from the lower conglomerate (unit IIa) and crater-fill deposits via the grey claystones (unit IIb) to the upper conglomerate (unit IIc).
3. An increase exists in medium-grained kaolinite in the conglomeratic unit IIc, compared to finer-grained kaolinite.

These relations indicate that clay minerals from unit I-type beds are the most likely sources of the clay minerals in the impactites of unit II. This sediment origin is also reflected in the overall mineralogical composition of the beds, as well as in their content of reworked, palynological fossils (Bremer et al. 2003; Smelror et al. 2001b). Sedimentary segregation in the coarse and fine-grained gravity flow deposits does not seem to have had a major effect on the variations in the clay mineral content or on the temperature differences and cooling rates within the cooling crater fill.

The chlorite detected in the impactites of units I and II most likely reflects reworked clastic chlorites from the underlying Triassic and Early Jurassic formations exposed and uplifted during the crater formation. However, kaolinite and illite could also have reacted with high temperature pore fluids to produce chlorite at depth, as is commonly observed in metamorphic environments. Subsurface temperatures at the impact site may have reached several thousand degrees locally and remained elevated at depth for a few Myr, accelerating such a mineral transformation. However, chlorite is present in these formations outside the Mjølnir region, especially the Early Triassic formations (Mørk et al. 2003), so the detrital origin is favored.

During the late Hekkingen post-impact time, chlorite may have reacted with acidic/sulphidic pore fluids returning to the crater, producing K and Fe-depleted illite and kaolinite. The clay mineral assemblage is most likely not in equilibrium, as seen in the number of illites present in the simulation. This is in contrast to the study of Jahren and Aagaard (1989), which show very limited variability in the illite composition in several reservoirs from the Norwegian shelf. In their paper, however, they show an example of the diagenetic alteration of chlorite to swelling chlorites, typically with an illitic phase. The higher abundance of a K-depleted, Fe-poor illite in the upper conglomerate (unit IIc) and closely adjacent underlying parts of the grey claystones (unit IIb) may reflect the effect of increased porewater percolation and alteration compared to the less permeable shales/claystone above and below. Consequently, we suggest that parts of the chlorite associated with the crater fill and chaotic sediments in the impact zone may have been altered to illite or kaolinite. The larger

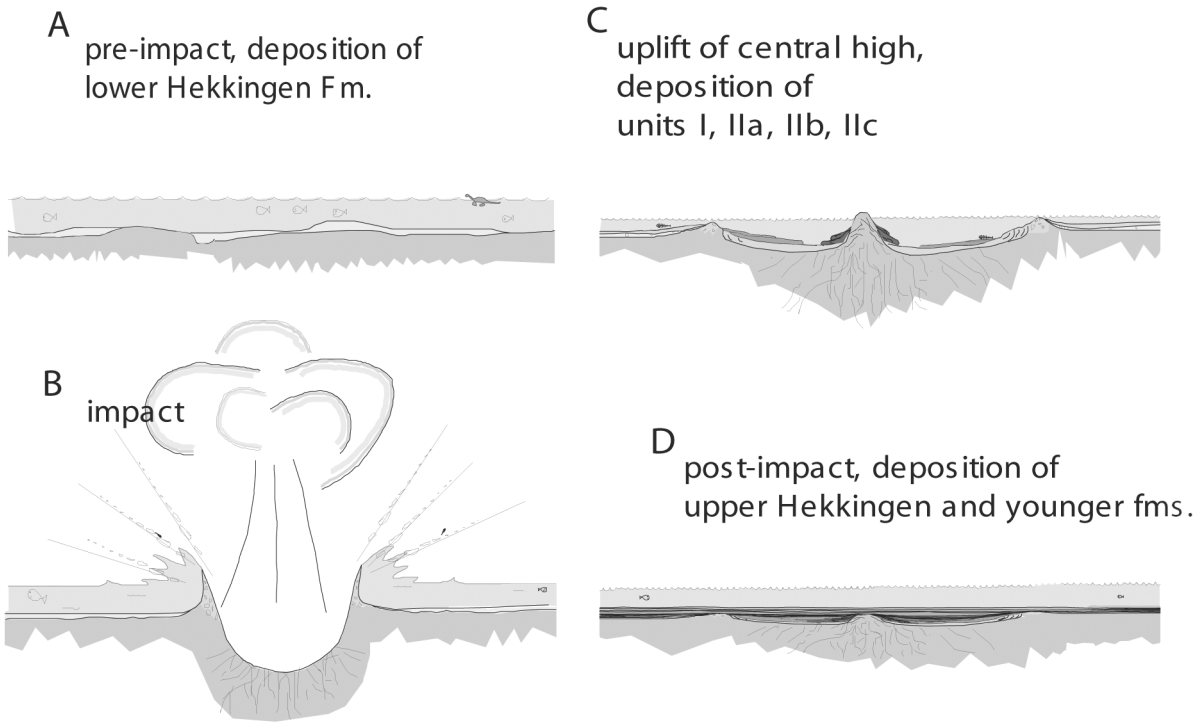

Fig. 10. A model for the sedimentary development of the Mjølnir crater.

quantities of ordered illite/smectite, mixed-layered clay minerals of vermiculitic affinity occurring in association with the upper conglomerates of unit IIc are a possible intermediate step in this reaction. They could also represent a phase that was formed as the illite adsorbed H_3O^+ from sea water, as presented below. The Fe-poor illite occurring in the last stage could be newly formed or transformed as K^+/H^+, increased due to dissolution of K-bearing phases and prolonged contact with percolating seawater.

chlorite + illite + H_3O^+ + sulphides → vermiculite + K-depleted illite → kaolinite + Fe-poor illite + pyrite

Segregation during sedimentation could produce an enrichment of kaolinite similar to that attributed to the chemical reactions above.

Note that medium-crystallite-size kaolinite is the dominant kaolinite in the upper conglomerates of unit IIc and is less dominant in the lower conglomerates (units IIa and IIb) where fine-crystallite-size and medium-crystallite-size kaolinite are subequal in abundance throughout the intervening grey claystones. Crystallite size is not an exact measure of particle size, but the two are typically correlated in a positive fashion. Thus, the greater abundance of the medium-crystallite-size kaolinite in unit IIc conglomerates could be a consequence of higher energy conditions in the depositional environment. The finer crystallite materials stayed in suspension and were transported further into the crater and winnowed from these sediments on the flanks of the central high. However, the medium crystallite kaolinite that is enriched in the more porous and permeable beds also possibly reflects a diagenetic kaolinite growth due to preferred alteration in those units compared to the less permeable shales and claystones below. This is supported weakly by their euhedral appearance and inverse abundance relative to chlorite. Consequently, we feel that the most likely origin of the medium-grained kaolinite is diagenetic growth at the expense of chlorite. The fine-grained kaolinite most likely reflects the clastic source and partial reworking of the pre-impact Jurassic and Triassic sediments. The coarse-crystallite kaolinite in the lower units is of mixed detrital and diagenetic origin. The impact of diagenesis, the destruction of chlorite, and the growth of kaolinite are not as pronounced in the more deeply buried deposits of the studied core.

Some of the illitic layers may have been stabilized with potassium from seawater and with hydroxides from chlorite destruction, forming the mixed-layered illite/smectite minerals and vermiculite/illte observed in the upper conglomerates. These reactions continued after normal sedimentary conditions returned to the area and are evident in the reduced chlorite content and the presence of a vermiculite/illite in the post-impact shale. The sediments of the Hekkingen Formation resulted from accumulation of fine-grained, highly weathered material. Thus, they are poorer in plagioclase and weakly enriched in potash feldspar, quartz, siderite, and pyrite compared to units below (Sandbakken 2002). They mark an important change from the reworking of the weakly metamorphosed chlorites and illites of the Middle Triassic to Lower Jurassic feldspar-bearing sediments below to the renewed Lower Cretaceous sedimentation of normal weathered sedimentary material.

The clay minerals in the claystones of unit IIb show only minor differences, compared to unit IIa below, (minor increase in kaolinite, decrease in illite of IIb compared to IIa) in the whole-rock analyses (Fig. 4). The mineralogy of these fine-grained claystones (unit IIb) show in thin section pyrite enrichments in their upper part, the same layers where anoxicity in the sediments are clearly shown by enrichments in elements such as V, Cr, Zn, and Ni (Dypvik et al. Forthcoming). This feature may indicate the return to marine, anoxic, depositional conditions in the impact crater. The presence of increased pyrite proportions continued into unit IIc and into the Hekkingen Formation above.

CONCLUSIONS

The most likely sequence of events recorded in the clay assemblage is a combined result of chemical and physical processes. The relative chlorite-rich sediment of unit II, with three varieties of illite and fine- to medium-crystallite-size kaolinite, was mainly created as a result of the reworking of sediments with a composition similar to unit I. Possibly, but less likely, a limited amount of chlorite and illite was formed by high temperature alteration of the seafloor sediments produced by the bolide impact. However, no clearcut evidence exists for this.

These relations establish a dominanly reworked origin for the clay minerals in the Ragnarok Formation. The clay minerals in the sediments of the overlying Hekkingen Formation resulted from weathering, erosion, transportation, and deposition of fine-grained suspended material in a marine basin, similar to the impact conditions that prevailed in the paleo-Barents Sea. The mineral content of these sediments from the central core of the crater was not changed by the impact.

During the impact, some minor amounts of impact glass were formed (Dypvik and Ferrell 1998). They have been found as smectitic alteration products of distal ejecta, but no glass particles have been found either in the Mjølnir core or the ejecta of core 7430/10-U-01. The newly-produced minerals and glass were ejected and suspended in the water and transported by currents radiating from the impact site and broadcasted over a wide area. Returning currents scoured the seafloor and may have created various gravity flow deposits. Some coarser, crystalline clays could have been enriched at this point, but we interpret most of the coarsely crystalline, euhedral kaolinite (KAO07) to have been formed by post-impact diagenesis that was more pronounced in the more porous and permeable beds than the surrounding claystones.

The clay minerals of the borehole inside the impact crater differ in two major ways from the clay minerals in the time-equivalent sediments of the nearby borehole 7430/10-U-01 (Dypvik and Ferrell 1998). The higher chlorite abundance in the samples from the central core reflects the reworking of older Jurassic and Triassic sediments. No clear-cut direct effects of higher temperatures or pressures that can be related to the impact were detected. The general scarcity of discrete smectite in the impact zone also reflects the likelihood that the glasses altered to smectite in the distal areas (well 7430/10-U-01) were either washed from the collapsing crater rim or, more likely, converted from ejecta glass. These results also underline the suggestion that only moderate amounts of glass, if any, were deposited within the upper parts of the Mjølnir Crater. This detailed clay mineralogical study of samples from the central high of a marine impact adds to the Ortega-Huertes et al. (1998) model for impactite clay mineralogy of ejecta and fireball material. In the impact crater, clay minerals are indicative of the original sediments underlying the impact site.

Acknowledgments–We would like to thank Wanda Le Blanc and Berit Løken Berg for technical asistance, the Mjølnir Project Group for fruitful cooperation, and the Norwegian Science Foundation for their financial support. The comments of Jeanne Percival and David Quint on an earlier version are highly appreciated.

Editorial Handling—Dr. Richard Grieve

REFERENCES

Aparicio P. and Ferrell R. E. 2001. An application of profile fitting and CLAY++ for the quantitative representation (QR) of mixed-layer clay minerals. *Clay Minerals* 36:501–514.

Bremer G. M. A., Smelror M., Nagy J., and Vigran J. O. 2003. Biotic responses to the Mjølnir meteorite impact, Barents Sea: Evidence from a core drilled within the crater. In *Cratering in marine environments and on ice,* edited by Dypvik H., Burchell M. J., and Claeys P. Heidelberg: Springer-Verlag. pp. 21–31.

Debrabant P., Fourcade E., Chamley H., Rocchia R., Robin E., Bellier J. P., Gardin S., and Thiebault F. 1999. Les argiles de la transition crétacé-tertiaire au Guatelame, témoins d'un impact d'astéroide. *Bulletin de la Société Géologique de France* 170:643–660.

Dypvik H. and Ferrell R. E. 1998. Clay mineral alteration associated with a meteorite impact in the marine environment (Barents Sea). *Clay Minerals* 33:51–64.

Dypvik H., Sandbakken P. T., Postma G., and Mørk A. Forthcoming. The post impact sedimentation in the Mjølnir Crater. *Sedimentary Geology.*

Dypvik H., Gudlaugsson S. T., Tsikalas F., Attrep M., Jr., Ferrell R. E., Jr., Krinsley D. H., Mørk A., Faleide J. I., and Nagy J. 1996. The Mjølnir structure: An impact crater in the Barents Sea. *Geology* 24:779–782.

Elliott W. C. 1993. Origin of the Mg-smectite at the Cretaceous/Tertiary (K/T) boundary at Stevns Klint, Denmark. *Clays and Clay Minerals* 41:442–452.

Gudlaugsson S. T. 1993. Large impact crater in the Barents Sea. *Geology* 21:291–294.

Huang K., Ferrell R. E., and Le Blanc W. S. 1993. Computer assisted interpretation of clay mineral XRD patterns (abstract). 30th Clay Minerals Society Annual Meeting. pp. 51.

Hughes R. E., Moore D. M., and Glass H. D. 1994. Qualitative and quantitative analysis of clay minerals in soils. In *Quantitative methods in soil mineralogy,* edited by Ammonette J. E. and Zelazny L. W. Madison: Soil Science Society of America. pp. 330–359.

Jahren J. S. and Aagaard P. 1989. Compositional variations in diagenetic chlorites and illites, and relationships with formation-water chemistry. *Clay Minerals* 24:157–170.

Kettrup B., Deutsch A., Ostermann M. and Agrinier P. 2000. Chicxulub impactites: Geochemical clues to the precursor rocks. *Meteoritics & Planetary Science* 35:1229–1238.

Leith T. L., Weiss H. M., Mørk A., Århus N., Elvebakk G., Embry A. F., Brooks P. W., Stewart K. R., Pchelina T. M., Bro E. G., Verba M. L., Danyushevskaya A., and Borisov A. V. 1993. Mesozoic hydrocarbon source-rock of the Arctic region. In *Arctic geology and petroleum potential,* edited by Vorren T. et al. NPF Special Publication 2. New York: Elsevier. pp. 1–25.

Martinez-Ruiz F., Ortega-Huertas M., and Palomo I. 2001. Climate, tectonics, and meteoritic impact expressed by clay mineral sedimentation across the Cretaceous-Tertiary boundary at Blake Nose, Northwestern Atlantic. *Clay Minerals* 36:49–60.

Mata P., Peacor D. R., Soria A. R., Lieae C., and Meléndez A. 2001. The spherule facies at the Cretaceous-Tertiary (K/T) boundary in the El Tecolote (northeastern Mexico): A TEM study. In *Impact markers in the stratigraphic record.* 6th ESF Impact Workshop, Granada, Spain. pp. 77–78.

Mørk M. B. E., Vigran J. O., Smelror M., Fjerdingstad V., and Bøe R. 2003. Mesozoic mudstone compositions and the role of kaolinite weathering: A view from shallow cores in the Norwegian Sea (Møre to Troms). *Norwegian Journal of Geology* 83:61–78.

Nyland B., Jensen L. N., Skagen J., Skarpnes O., and Vorren T. 1992. Tertiary uplift and erosion in the Barents Sea: Magnitude, timing, and consequences. In *Structural and tectonic modelling and its application to petroleum geology,* edited by Larsen R. M., Brekke H., Larsen B. T., Talleraas E. Proceedings, NPF Special Publication 1. New York: Elsevier. pp. 153–162.

Ortega-Huertas M., Martines-Ruiz F., Palomo I., and Chamley H. 2002. Review of the mineralogy of the Cretaceous-Tertiary boundary clay: Evidence supporting a major extraterrestrial catastrophic event. *Clay Minerals* 37:395–411.

Ortega M., Palomo I., Martines-Ruiz F., and González I. 1998. Geological factors controlling clay mineral patterns across the Cretaceous-Tertiary boundary in Mediterrean and Atlantic sections. *Clay Minerals* 33:483–500.

Palmer B. A., Alloway B. V., and Neall V. E. 1991. Volcanic-debris-avalanche deposits in New Zealand: Lithofacies organization in unconfined, wet-avalanche flows. In *Sedimentation in volcanic settings,* edited by Fisher R. V., and Smith G. A. Special Publication 45. Tulsa: SEPM, Society for Sedimentary Geology. pp. 89–98.

Pollastro R. M. and Bohor B. F. 1993. Origin and clay mineral genesis of the Cretaceous-Tertiary boundary unit, western interior of North America. *Clays and Clay Minerals* 41:7–25.

Robert C. and Chamley H. 1990. Paleoenvironmental significance of clay mineral associations at the Cretaceous-Tertiary passage. *Paleogeography, Paleoclimatology, Paleoecology* 79:205–219.

Sandbakken P. T. 2002. A geological investigation of the Mjølnir crater core (73219/03-U-01), with emphasis on shock metamorphosed quartz. Cand Scient (M.Sc.) Thesis, University of Oslo, Oslo, Norway. 142 p.

Shuvalov V. and Dypvik H. Forthcoming. Ejecta formation and crater

development of the Mjølnir impact. *Meteoritics & Planetary Science*.

Shuvalov V., Dypvik H., and Tsikalas F. 2002. Numerical simulations of the Mjølnir marine impact crater. *Journal of Geophysical Research* 107:1.11–1.13.

Smelror M., Mørk M. B. E., Mørk A., Løseth H., and Weiss H. M. 2001a. Middle Jurassic-lower Cretaceous transgressive-regressive sequences and facies distribution off Troms, Northern Norway. In *Sedimentary environments offshore Norway—Palaeozoic to recent,* edited by Martinsen O. J. and Dreyer T. Special Publication 10. Stavanger: Norwegian Petroleum Society. pp. 211–232.

Smelror M., Kelly S. R. A., Dypvik H., Mørk A., Nagy J., and Tsikalas F. 2001b. Mjølnir (Barents Sea) meteorite impact offers a Volgian-Ryazanian boundary marker. *Newsletter on Stratigraphy* 38:129–140.

Smit J. 1999. The global stratigraphy of the Cretaceous-Tertiary boundary impact ejecta. *Annual Review of Earth and Planetary Sciences* 27:75–133.

Tsikalas F., Gudlaugsson S. T., and Faleide J. I. 1998. The anatomy of a buried complex impact structure: The Mjølnir structure, Barents Sea. *Journal of Geophysical Research* 103:30469–30483.

Tsikalas F., Gudlaugsson S. T., Faleide J. I., and Eldholm O. 1999. Mjølnir structure, Barents Sea: A marine impact crater laboratory. Geological Society of America Special Paper 339. pp. 193–204.

Weaver C. E. 1989. Clays, mud, and shales. In *Developments in Sedimentology 44*. New York: Elsevier. 819 p.

Wolbach W., Widicus S., and Dypvik H. 2001. A preliminary search for evidence of impact-related burning near the Mjølnir impact structure, Barents Sea (abstract #1332). 32nd Lunar and Planetary Science Conference.

Worsley D., Johansen R., and Kristensen S. E. 1988. The Mesozoic and Cenozoic succession of Tromsøflaket. In *A lithostratigraphic scheme for the Mesozoic and Cenozoic succession offshore mid- and northern Norway,* edited by Dalland A., Worsley D., and Ofstad K. Norwegian Petroleum Directorate Bulletin 4. Stavanger: Oljedirektoratet. pp. 42–65